Diffusion and Reaction in Fe-Based Catalyst for Fischer-Tropsch Synthesis Using Micro Kinetic Rate Expressions

Arvind. Nanduri[1] and Patrick L. Mills[*1]
[1]Texas A&M University-Kingsville, Department of Chemical & Natural Gas Engineering
*Corresponding author: Texas A&M University-Kingsville, Department of Chemical & Natural Gas Engineering, EC 303D, MSC 193, Kingsville, TX-78363-8202, USA. Email: Patrick.Mills@tamuk.edu

Abstract: A 1-D catalyst particle model for three different shapes (cylinder, sphere and hollow cylinder) was numerically simulated to analyze the particle-level performance for the Fischer-Tropsch Synthesis (FTS). A Fe-based micro-kinetic olefin re-adsorption model developed by Wang *et al*. (2008) was coupled with the Soave-Redlich-Kwong (SRK) equation of state to describe the particle-scale transport-kinetic interactions and phase behavior for the gas-phase FTS [3]. The intra-particle effectiveness factor, liquid-to-vapor ratio, CO conversion and intra-particle methane-based diesel selectivity were analyzed at different process conditions to compare the performance of the different catalyst particle shapes.

Keywords: catalyst particle shape, Fischer-Tropsch Synthesis, vapor-liquid-equilibrium (VLE), gas phase micro-kinetics.

1. Introduction

Fischer-Tropsch Synthesis (FTS) is a highly exothermic polymerization reaction of syngas ($CO+H_2$) in the presence of Fe/Co/Ru-based catalysts to produce a wide range of paraffins, olefins and oxygenates, which is often called *syncrude*. Multi-Tubular Fixed Bed Reactors (MTFBR) and Slurry Bubble Column reactors (SBCR) are widely employed for FTS processes [1]. To understand the reactor-scale catalyst performance, it is important to first study the particle-scale transport-kinetic interactions.

The FTS is a polymerization reaction producing hydrocarbons with carbon numbers ranging from 1 to 100 so the catalyst pores in this process will be filled with liquid wax (C_{20}+) leading to high diffusional limitations. To comprehensively model such a reaction network, micro-kinetic rate expressions for each individual species must be coupled with the intraparticle solubility of gases in liquid wax and transport equations for the various reaction species in the porous catalyst.

2. Catalyst Pellet Model

The isothermal 1-D catalyst pellet model used to describe transport-kinetic interactions is presented in this section.

A total number of 20 paraffins (C_1 to C_{20}), 19 olefins (C_2 to C_{20}) and 4 key components (H_2, CO, CO_2, and H_2O) are considered in the reaction network, which leads to 43 nonlinear differential equations for the specie mass balances. The micro-kinetic and thermodynamic expressions used in the model can be found elsewhere [2-4]. Three different particle shapes (cylinder, sphere, and hollow cylinder) of equal volume are simulated in this paper. The catalyst shapes are illustrated in Figure 1.

2.1 Specie mass balance equations

The specie mass balance equations for each particle shape are summarized below.

Spherical pellet:

$$\frac{1}{\xi^2}\frac{\partial}{\partial\xi}\left(D_{ei}\xi^2\frac{\partial C_i}{\partial\xi}\right) = -\rho_p {R_p}^2 \sum_j \alpha_{ij} R_{ij}$$

$$\xi = \frac{r}{R_p}$$

Cylindrical pellet:

$$\frac{1}{\xi}\frac{\partial}{\partial\xi}\left(D_{ei}\xi\frac{\partial C_i}{\partial\xi}\right) = -\rho_p {R_p}^2 \sum_j \alpha_{ij} R_{ij}$$

$$\xi = \frac{r}{R_p}$$

Hollow cylinder:

$$\frac{1}{(\xi\delta + R_i)}\frac{\partial}{\partial\xi}\left((\xi\delta + R_i)D_{ei}\frac{\partial C_i}{\partial\xi}\right)$$

$$= -\rho_p \delta^2 \sum_j \alpha_{ij} R_{ij}$$

$$\xi = \frac{r - R_i}{R_o - R_i}$$

$$\delta = R_o - R_i$$

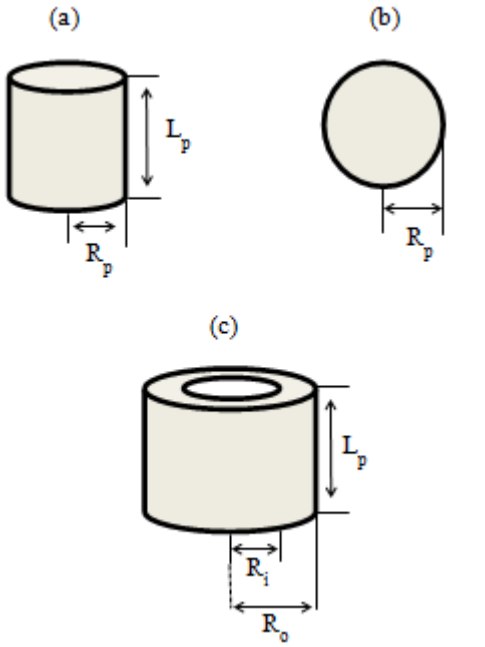

Figure 1. Catalyst particle shapes. (a) cylinder, (b) sphere, and (c) hollow cylinder

2.2 Boundary conditions

The boundary conditions correspond to specified concentrations at the pellet surface (Dirichlet conditions).

Spherical pellet:

At ξ = -1 and ξ = 1, $C_i = C_{i,bulk}$

Cylindrical pellet:

At ξ = -1 and ξ = 1, $C_i = C_{i,bulk}$

Hollow cylinder:

At ξ = 0 (inside surface) and ξ = 1 (outside surface), $C_i = C_{i,bulk}$

2.3 Vapor-Liquid-Equilibrium calculations

The vapor-liquid equilibrium for the FTS reaction mixture is described by the Soave-Redlich- Kwong equation of state [3]. The flash calculations are based upon satisfying the Rachford-Rice objective function:

$$F(\alpha_g) = \sum_i \frac{z_i(K_i - 1)}{\left(1 + \alpha_g(K_i - 1)\right)} = 0$$

In this application, the Rachford-Rice objective function is a polynomial of degree 43 (43 distinct roots). Since the fraction α_g = V/(V+L) is a positive number less than 1, only the roots that make physical sense are considered. The initial estimate of the distribution coefficient is obtained from Wilson's correlation [3]:

$$K_i^{\text{guess value}} = \frac{P_{ic}}{P} \exp\left(5.37(1 + \omega_i)\left(1 - \frac{T_{ic}}{T}\right)\right)$$

Here, the distribution coefficient is defined as the ratio of the vapor to liquid mixture fugacity coefficients:

$$K_i = \frac{\emptyset_i^V}{\emptyset_i^L}$$

3. Use of COMSOL Multiphysics

The 1-D diffusion-reaction system was solved using the transport of diluted species module in COMSOL Multiphysics assuming steady-state conditions. The Rachford-Rice objective function (VLE calculations) was solved using the coefficient form of the PDE solver. The catalyst properties and operating conditions used in the models are listed in Tables 1 - 4. The solution for the specie concentration profiles were based upon a convergence factor of 10^{-3}.

To avoid convergence issues, the particle radius was set to a small number (0.01 mm) and the subsequent solution was used as initial conditions for higher values of the particle radius until R_p = 1.5 mm was reached . This was performed by doubling the previous value of the radius. Since the FTS is a relatively fast diffusion-reaction system, numerical instabilities were encountered in the interior region of the particle as the CO and CO_2 concentrations approached zero. The convergence issues were

solved by using built-in logical operators, such as CO = if(CO ≤ 0,eps,CO), and CO_2 = if(CO_2 ≤ 0,eps,CO_2) which resulted in positive values for the specie concentrations. Mesh refinement was manually performed until the concentration profiles were relatively constant and satisfied the convergence criterion.

Table 1. Cylinder and ring dimensions that produce a sphere whose volume is based on a of radius 1.5 mm

Cylinder	L_p = 3 mm & R = 1 mm
Ring	L_p = 2 mm, R_o= 1.5 mm & R_i= 0.3 mm

Table 2. Cylinder and ring dimensions that produce a sphere whose volume is based on a of radius 1 mm

Cylinder	L_p = 3 mm & R = 0.7 mm
Ring	L_p = 2 mm, R_o= 1.5 mm & R_i= 1 mm

Table 3. Catalyst properties

Density of pellet, ρ_p	1.95 x 10^6 (gm/m^3)
Porosity of pellet,ε	0.51
Tortuosity, τ	2.6

Table 4. Operating conditions.

Temperature, ^oK	493, 523 & 533
Pressure, bar	20, 25 & 30
H_2/CO	2

4. Results

4.1 Concentration profiles of key components

The 1-D isothermal concentration profiles of the key components (H_2, CO, CO_2 and H_2O) for different catalyst particle shapes are shown in Figure 2 - 4. The profiles show that the CO concentration approaches zero for all shapes due to the presence significant diffusional limitations. The CO_2 concentration reaches a peak and then decreases due to the reverse Water-Gas-Shift (WGS) reaction. The reverse WGS reaction produces CO, which is then consumed in the subsequent hydrocarbon producing FT reactions.

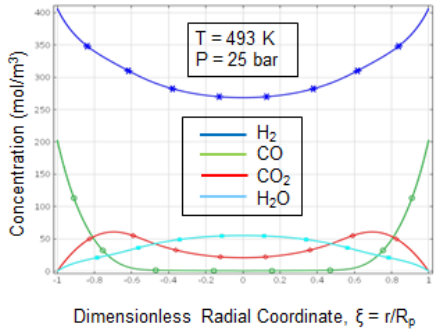

Figure 2. Concentration profiles of key components in a cylindrical pellet with a radius R_p = 1 mm.

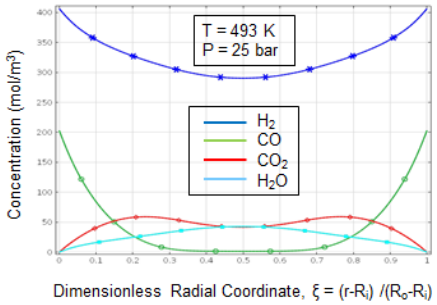

Figure 3. Concentration profiles of key components in a ring pellet with an external radius R_o = 1.5 mm and an internal radius R_i = 1.2 mm.

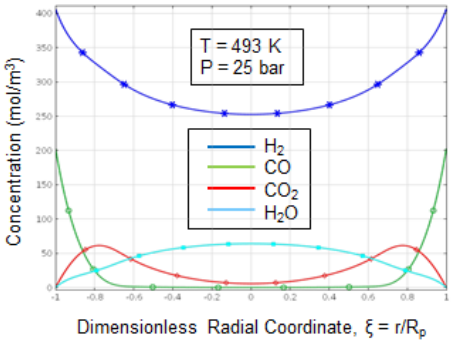

Figure 4. Concentration profiles of key components in a spherical pellet with a radius R_p = 1.5 mm.

4.2 Intra-particle effectiveness factor

The intra-particle effectiveness factor (η) for different particle shapes are shown in Figure 5, - 7. The effectiveness factor has a decreasing trend

with temperature and as the center of the particle is approached.

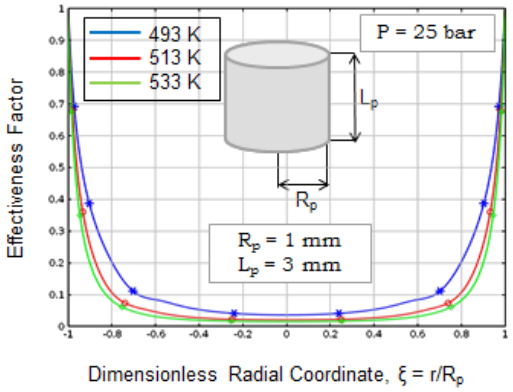

Figure 5. Intra-particle effectiveness factor of a cylindrical catalyst pellet at different temperatures.

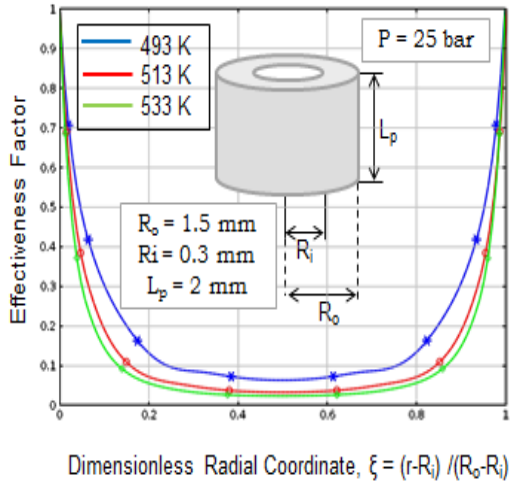

Figure 6. Intra-particle effectiveness factor of a ring catalyst pellet at different temperatures.

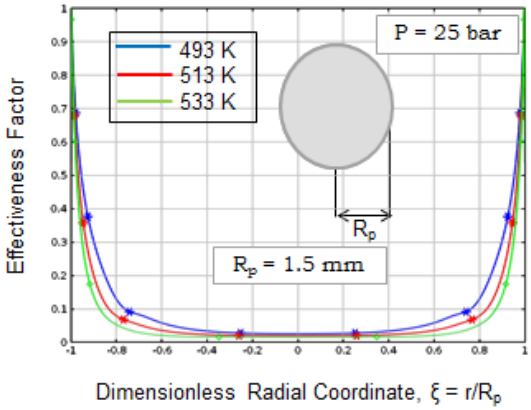

Figure 7. Intra-particle effectiveness factor of a spherical catalyst pellet at different temperatures.

4.3 Intra-particle liquid-to-vapor ratio

The intra-particle liquid-to-vapor molar ratio (L/V) for different particle shapes is shown in Figure 8 - 10. These results show that the ring and hollow cylinder particles have the smallest liquid fraction while the spherical catalyst pellet has the maximum. This result is also supported by comparing concentration profiles of key components (see Figures 2 - 4) where the spherical particle exhibits the most significant diffusional limitation. These results also show the importance of understanding the phase behavior of FT products in the catalyst pores since the reaction kinetics for liquid phase and gas phase would differ.

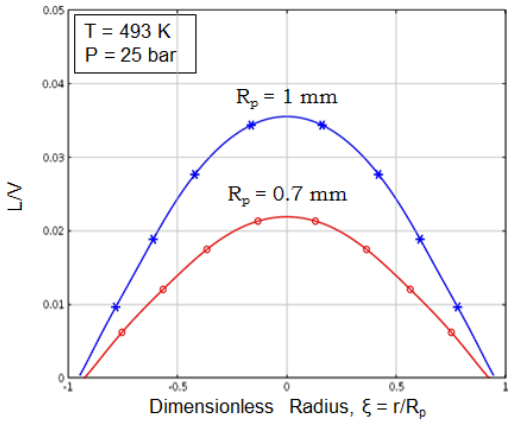

Figure 8. Intra-particle liquid-to-vapor ratio for a cylindrical catalyst pellet.

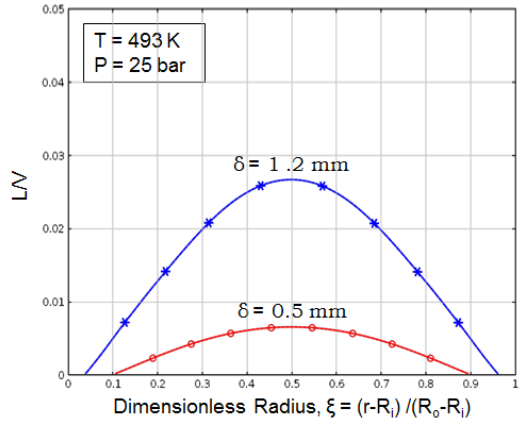

Figure 9. Intra-particle liquid-to-vapor ratio for a ring catalyst pellet.

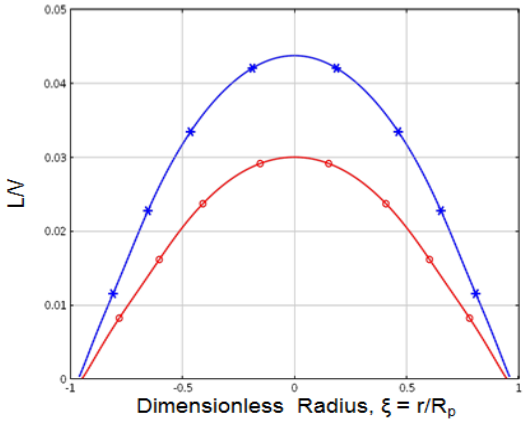

Figure 10. Intra-particle liquid-to-vapor ratio for a spherical catalyst pellet.

4.4 Intra-particle methane-based diesel selectivity

The intra-particle methane-based diesel selectivity ($S_{i,CH4}$) for different particle shapes are shown in Figures 11 - 13. Both the ring and spherical catalyst particle shapes have higher diesel selectivity when compared to that of a cylindrical catalyst particle. The hollow ring may have a lower mechanical strength than the other two shapes which would require additional considerations that are outside the scope of this study.

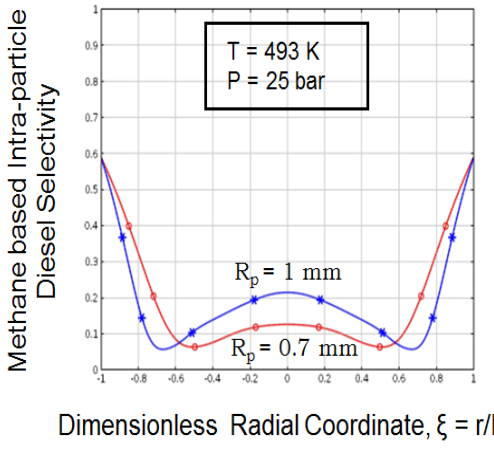

Figure 11. Intra-particle methane-based diesel selectivity for a cylindrical catalyst pellet.

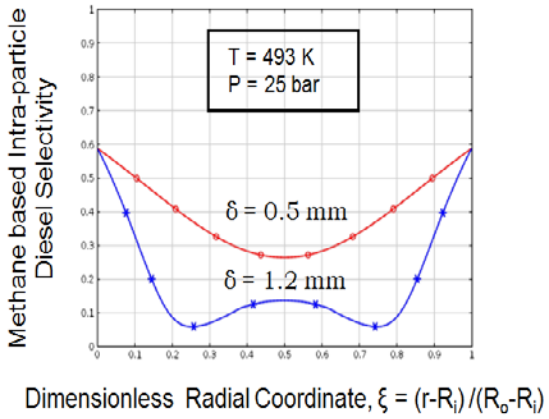

Figure 12. Intra-particle methane-based diesel selectivity for a ring catalyst pellet.

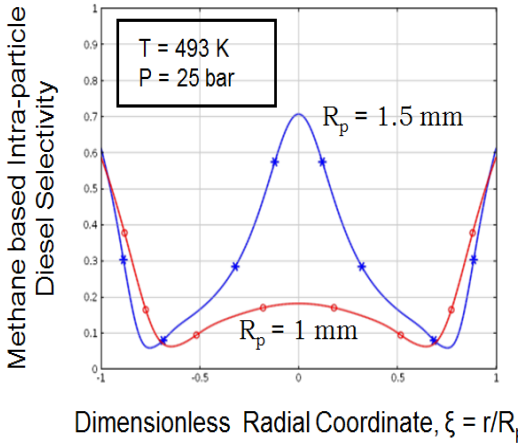

Figure 13. Intra-particle methane-based diesel selectivity for a spherical catalyst pellet.

5. Conclusions

The transport-kinetic interactions for FTS in a 1-D catalyst pellet model using a detailed micro-kinetic model were successfully analyzed for the first time using COMSOL Multiphysics. Previous work by Wang *et al*. (2008) used the same micro-kinetic model, but did not report the methane-based diesel selectivity or the corresponding liquid-to-vapor molar ratios. Also, the numerical technique was based upon a custom computer code that implemented the orthogonal collocation method for the two point boundary value system of ODEs. The results in the current work will provide the basis for modeling the catalyst bed using the packed bed reactor model in COMSOL Multiphysics 5.0.

6. Nomenclature

C_i	Concentration of species 'i' (mol/m^3)
$C_{i,bulk}$	Concentration of species 'i' in bulk phase (mol/m^3)
D_{ei}	Effective diffusivity of species 'i' (m^2/s)
K_i	Equilibrium ratio
L	Number of moles in the liquid phase (moles)
L_p	Length of catalyst pellet (mm)
P	Pressure (bar)
P_{ic}	Critical pressure of component i (bar)
r	Radial coordinate (mm)
R_p	Radius of catalyst pellet (mm)
R_i	Internal radius of hollow cylinder (mm)
R_o	External radius of hollow cylinder (mm)
R_{ij}	Rate of component i in j^{th} reaction ($mol\ kg^{-1}\ s^{-1}$)
$S_{i,CH4}$	Methane-based diesel selectivity ($\frac{\sum_{i,j}\alpha_{ij}R_{ij}}{\sum_{CH_4,j}\alpha_{CH_4,j}R_{CH_4,j}}$)
T	Temperature (K)
T_{ic}	Critical temperature of component i (K)
V	Number of moles in vapor phase
z_i	Number of moles of component i

Greek Letters

α_g	Intra-particle vapor fraction
α_{ij}	Stoichiometric coefficient of component i in reaction j
ξ	Radial coordinate, dimensionless
δ	Thickness of ring/hollow cylinder (mm)
η	Intra-particle effectiveness factor ($\frac{\sum_{i,j}\alpha_{ij}R_{ij}}{(\sum_{i,j}\alpha_{ij}R_{ij})_{max}}$)
ρ_p	Density of catalyst pellet (kg/m^3)
ε	Catalyst pellet porosity
τ	Catalyst tortuosity

7. References

1. D. A. Wood, C. Nwaoha, and B. F. Towler, Gas-To-Liquids (GTL): A Review of an Industry Offering Several Routes for Monetizing Natural Gas, *Journal of Natural Gas Science and Engineering*, **9**, 196-208 (2012)

2. Yi-Ning Wang, Yuan-Yuan Xu, Hong-Wei Xiang, Yong-Wang Li, and Bi-Jiang Zhang, Modeling of Catalyst Pellets for Fischer-Tropsch Synthesis, *Industrial & Engineering Chemistry Research*, **40**, 4324-4335 (2001)

3. Y. N. Wang, Y. W. Li, L. Bai, Y. L. Zhao, and B. J. Zhang, Correlation for Gas-Liquid Equilibrium Prediction in Fischer-Tropsch Synthesis, *Fuel*, **78**, 911-917 (1999)

4. Yi-Ning Wang *et al.*, Kinetic Modelling of Fischer-Tropsch Synthesis Over an Industrial Fe-Cu-K Catalyst, *Fuel*, **82**, 195-213 (2003)